Polymer structures for photovoltaics using colloidal self-assembly, thermal nanoimprinting and electrohydrodynamic annealing

Master's thesis within the Master of science
in engineering physics programme
Umeå University

Ivan Huuva
ivanhuuva@gmail.com

Supervisor: David Barbero
Examiner: Magnus Andersson

June 2012

Abstract

The efficiency of an organic photovoltaic cell depends mainly on its morphology where an exciton has to migrate to a p-n junction to create a photocurrent. Therefore the distance from the bulk of the cell to a junction interface should not exceed the diffusion length of the exciton. In this thesis, two novel lithographical methods, to produce specific polymer morphologies, were developed and evaluated. In the first method, called *embedded annealing*, self-assembled polystyrene colloids were embedded in a polydimethylsiloxane (PDMS) film and annealed under an electric field to produce a bi-polymer structure consisting of polymer columns in a thin film of PDMS. Polymer colloids were successfully assembled into two dimensional hexagonally close packed arrays. However, the annealing process was unsuccessful. The second method, *imprint annealing*, aimed to increase the aspect ratio (height/width) of thermally imprinted micrometer sized polystyrene features by annealing them in uniform electric fields. The results showed that the aspect ratio of imprinted features can be significantly increased, 21-fold, while maintaining the periodicity of the original imprint. This is in contrast to previous results where smooth polymer films annealed in uniform fields where the periodicity of the resulting structures cannot be independently controlled, and are highly sensitive to the electrode spacing. Feature sizes down to 1 m and aspect ratios up to 4.5 were achieved using *imprint annealing*.

Sammanfattning

Verkningsgraden hos en hos en solcell beror, för givna material, framförallt på dess uppbyggnad. För att bidra till fotoströmmen måste en genererad exciton vandra till en p-n övergång. På grund av detta bör det längsta avståndet till närmaste p-n-övergång i solcellen inte vara längre än excitonens diffusionslängd. I detta examensarbete testas två olika litografiska metoder för att åstadkomma en specifik filmgeometri lämpad för organiska solceller. Den första metoden, kallad *embedded annealing*, går ut på att bädda in spontant ordnade sfäriska polystyrenkolloider i en polydimetylsiloxan (PDMS) -film för att sedan vid förhöjd temperatur applicera ett elektiskt fält över filmen. Förhoppningen var att på detta sätt töja ut kolloiderna till pelare genom PDMS-filmen. I det första steget ordnades kolloiderna sponant i tätpackade hexagonala tvådimensionella gitter på kiselsubstrat. Experimenten lyckades inte med hjälp av elektriska fält töja ut kolloiderna. Den andra metoden, *imprint annealing*, syftar till att öka höjd/bredd -förhållandet och minska diametern hos präglade polystyrenstrukturer. Dessa ursprungliga topografiska stukturer skapas med hjälp av en tryckpressmetod kallad nanoimprinting. Dessa strukturer värmdes upp, och ett uniformt elekrisk fält applicerades över dem. Mina resultat visar att man med elektriska fält avsevärt kan öka höjd-breddförhållandet hos polymerstrukturer och samtidigt bevara periodiciteten hos de ursprungliga strukturerna. Detta står i kontrast mot tidigare resultat på släta filmer, där periodiciteten inte kan kontrolleras oberonde av andra parametrar. Med *imprint annealing* ökades höjd-breddförhållandet hos enskilda strukturer upp till 21 gånger. Diametrar ner till 1 μm och höjd/breddförhållanden upp till 4,5 uppnåddes.

Contents

1 Introduction **5**

2 Background and review of methods **7**
2.1 Colloidal Crystals 7
2.1.1 Structure and applications 7
2.1.2 Characterization of colloidal crystals 8
2.2 Fabrication of colloidal crystals 9
2.2.1 Solvent evaporation assisted self-assembly 9
2.2.2 Self-assembly at an interface 10
2.2.3 Self-assembly during spin coating 12
2.2.4 Methods of choice 13
2.3 Electrohydrodynamic Patterning 13

3 Experimental **15**
3.1 Wedge cell assembly 15
3.2 Assembly by floating 16
3.3 Electrohydrodynamic experiments 18
3.3.1 Experimental set up and materials 18
3.3.2 Embedded annealing 19
3.3.3 Imprint annealing 21
3.4 Characterization 24

4 Results **25**
4.1 Wedge cell assembly 25
4.2 Self-assembly by floating 29
4.3 Embedded annealing 30
4.4 Imprint annealing 33

5 Conclusion **40**

References **40**

A Conditions for imprint annealing experiments **45**

List of Figures

2.1 Solvent evaporation assisted self-assembly 9
2.2 EHD Schematic 14

3.1 Wedge shaped cell used for evaporation assisted self-assembly 16
3.2 Schematic of colloidal assembly by floating 17
3.3 Schematic of EHD set up 19
3.4 Polystyrene spin curves 22
3.5 AFM images and height profiles of molds 23

4.1 Colloids assembled on a silicon substrate 25
4.2 Monolayers produced with the wedge cell method 27
4.3 Monolayers produced with the floating method 30
4.4 AFM scan of annealed sample 32
4.5 SEM images of PDMS embedded colloids after annealing . . . 32
4.6 Optical micrographs of annealed imprints at electrode edge . . 34
4.7 Pillar diameters 35
4.8 Optical micrographs of annealed imprints 35
4.9 Pillar heights 36
4.10 Pillar aspect ratios 36
4.11 Imprint before and after annealing 37
4.12 AFM profile of 1.9 μm features 38
4.13 Optical micrograph of annealed 1.9 μm features 39

List of Tables

4.1 Optical micrographs of wedge cell assembly experiments . . . 28
4.2 Embedded annealing conditions 31

A.1 Experimental conditions and comments for annealed samples imprinted using molds with 4 μm diameter holes 46
A.2 Experimental conditions and comments for annealed samples imprinted using molds with 4 μm diameter holes, continued . 47
A.3 Experimental conditions and comments for annealed samples imprinted using molds with 4 μm diameter holes, continued . 48
A.4 Experimental conditions and comments for annealed samples imprinted using molds with 1.9 μm wide pyramidal holes . . . 49

Chapter 1

Introduction

The need for renewable energy

There is a common consensus in the global scientific community that a change in the energy consumption of the world is needed. To avoid, or at least alleviate, the negative environmental consequences of the global economy, a shift towards renewable carbon neutral energy sources is necessary [1]. Another motivation for the development of new energy harvesting technologies are the prospects that the oil- and natural gas production volume of the world may reach a maximum within decades [2, 3].

If production levels are to be maintained during a shift like this, enormous quantities of fossil fuels have to be replaced with renewable alternatives. Currently no single alternative source is a realistic substitute in terms of volume, and a broad mix of renewables will have to be employed. Photovoltaics (PV) are currently a small contributor, but new solar cells based on organic materials hold promise for reducing the cost of production significantly, thus making PV an alternative to fossil fuels to be reckoned with in many areas [4]. While organic PV have come some way, a lot still needs to be done in increasing their efficiency.

Photovoltaic cells

The operation of PV-cells is based on semiconductors. Electrical current in semiconductors is carried by electrons and/or holes. When the main charge carrier is electrons, the semiconductor is called n-type. When current is instead mainly carried by holes, the material is called p-type. A boundary between n-type and p-type material has a built in voltage drop and is called a p-n junction. In PV-cells, excitons are generated in the semiconductor by incoming photons. The excitons are of neutral charge, but if they diffuse to a p-n junction they can be separated by the built in voltage and give rise to a

photocurrent as the electron and the hole are collected at opposite electrodes connected to the solar cell. Traditionally, PV-cells of this kind have been made from inorganic semiconductors, most often silicon. In the last few decades however, PV-cells have been developed from conductive polymers. Conductive polymers also come in p- and n-type varieties, and the operation of organic bilayer PV-cells is based on a p-n junction as described above. The main advantage of organic solar cells is their potentially low production cost compared to silicon PV-cells, but they are still hindered by low efficiency [5].

The morphology of a photovoltaic cell

One way of increasing the efficiency of an organic bilayer PV-cell is to control the morphology of the cell. As mentioned above an exciton needs to migrate to a p-n junction to be dissociated and collected. All excitons that do not reach a junction contribute to the losses of the solar cell. The average exciton diffusion length in the polymers used is very small (in the order of ten nanometers), and because of this, devices must be carefully designed to maximize the number of photo-generated excitons that reach the junction interface [5].

A specific bi-polymer geometry well suited for PV applications is a thin film of one polymer penetrated by an array of pillars of another polymer. If the two polymers used are donor- and acceptor materials, the lateral surface of each pillar then comprises a junction interface, at which charge separation can occur. By tuning the size of the pillars and the distance between them, one can optimize the device for a specific diffusion length.

Aim of project

This project introduces and tests two novel methods for producing this arrays of pillars, both making use of electrohydrodynamic (EHD) annealing of polymers. In the first of the methods, self assembled polymer colloids are embedded in another polymer. Annealing of the embedded colloids in an electric field is expected to produce the desired bi-polymer geometry. This method will from now on be called *embedded annealing*.

The other method, from now on referred to as *imprint annealing*, uses a single polymer. The aim is to increase the aspect ratio of imprinted features of the polymer forming the pillars by EHD annealing. The obtained structure can be viewed as a precursor to the bi-polymer geometry described. The possibility of increasing the aspect ratio of polymer features by EHD is also novel, as it has not, to the knowledge of the author, been demonstrated before.

Chapter 2

Background and review of methods

2.1 Colloidal Crystals

An intricate step of the *embedded annealing* is the deposition of the colloids. The colloids should be in a monolayer with well defined interparticle distance and, if possible, in a well defined array. Colloids, if deposited in a two dimensional (2D) array, can be regarded as a 2D colloidal crystal.

In the following paragraphs the research on colloidal crystals and their fabrication, relevant to this project, will be reviewed. First a brief introduction to the subject is given, after which the methods of characterization of samples and a number of different fabrication approaches are presented. Finally, conclusions are drawn as to which methods show most promise to fit the needs of this project.

2.1.1 Structure and applications

Colloidal crystals, highly ordered structures built up from nano- to micrometer sized particles, have in recent years attracted a lot of attention. The crystals are also commonly referred to as photonic crystals if they consist of dielectric nanoparticles or artificial opals. The former denomination is due to the fact that these crystals have a lattice spacing on the order of the wavelength of visible light, which makes the propagation of light in them analogous to that of electrons in atomic crystals [6]. The latter denomination is used because naturally occurring opals consist of ordered arrays of fairly monodisperse silica nanospheres, making them an example of a natural colloidal or photonic crystal.

Usually colloidal crystals are prepared from highly monodisperse silica or polystyrene colloids, with methods that can in principle be applied to a wide variety of colloids. The prevalence of silica and polystyrene colloids is mainly due to their high commercial availability and comparatively low cost. Silica colloids are usually synthesized in the Stöber process, while polymer colloids are typically synthesized in emulsion polymerization processes [7].

Self assembled colloidal crystals have been produced to varying degree of perfection by a number of methods. For the application in mind, it is crucial that the crystals produced are 2D, that is that they are monolayers. Some of the research covered below targets the production of 2D crystals exclusively. Other methods, though used for 3D crystals, may allow for the production of 2D crystals as a special case by tuning for example the concentration of colloids in the master solution.

2.1.2 Characterization of colloidal crystals

To assess the merits of different approaches in the production of colloidal crystals one needs to characterize produced samples. Microscopic imaging is the most commonly used characterization method, and optical microscopy or scanning electron microscopy (SEM) images of reportedly representative sections of the crystals are usually presented in the publications. The thickness of crystals is usually determined from profile views of these images.

As a further indication of the crystalline quality, images captured normal to a crystalline plane are often accompanied by their Fast Fourier Transforms (FFT), as generated by image analysis software such as ImageJ [8]. However, the FFT images still only give a qualitative sense of the crystalline quality, and applies only to the small portion of the top plane covered in the microscopic image. This method is therefore extremely laborious to use for characterization of centimeter sized samples, and different sampling methods are sometimes used [9].

Another commonly used method is that of normal incidence transmission or reflectivity spectra, where well defined Bragg peaks indicate a high degree of ordering [9, 10, 11]. These methods have the advantage that they readily allow larger area scans, but they give no details on the nature of the crystalline imperfections. Another method, used for 2D-crystals, that gives information comparable to the FFT images but more easily lends itself to scanning of larger areas is laser diffraction [12, 13]. Still, the lack of a universally accepted method of quantifying the quality of produced crystals remains a problem when comparing the the merits of different publications.

2.2 Fabrication of colloidal crystals

2.2.1 Solvent evaporation assisted self-assembly

The most common approaches to colloidal crystal self-assembly are based on the fact that when the solvent of a colloidal suspension evaporates, convective flow transports colloids from the bulk of the suspension and deposits them at the drying front - a three phase contact line. An everyday manifestation of this phenomenon is the ring deposited at the periphery of a dried coffee stain, and it is aptly called the coffee ring effect [14]. It has been found that the process can be tuned so that the colloids transported to the drying line spontaneously self-assemble into a hcp lattice structure, given that the colloids are spherical, sufficiently monodiperse and that the substrate surface is smooth and clean enough. The assembly is mainly driven by capillary forces [15, 16, 17, 18, 19].

Relatively high ordering has been achieved using a process where a substrate is placed vertically in a colloidal suspension that evaporates in a controlled fashion, see figure 2.1. Still, defects are abundant, and a varying thickness profile of the resulting crystal has been claimed intrinsic to the process, although a closely related method used in other work reportedly produces highly controlled constant thickness and a very low defect ratio [20, 9]. Different methods of characterization however make comparison of the results difficult.

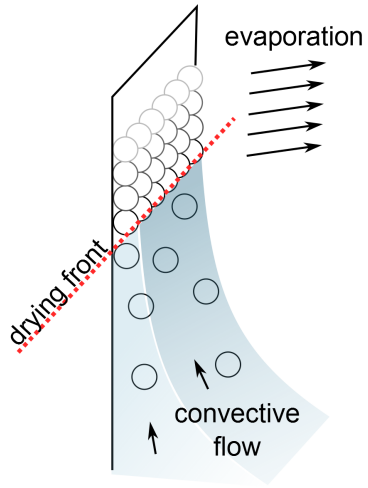

Figure 2.1: A schematic of the solvent evaporation assisted self-assembly process

Suspension concentration and meniscus shape

A number of papers have addressed the question of how to control the thickness and quality of the produced colloidal crystals. The conclusions are that the evaporation rate, the shape of the meniscus at the drying front and the concentration of the suspension all play a role [18, 21, 22]. A steeper (sharper) meniscus or a lower concentration both result in thinner crystals, while the evaporation rate mainly effects the quality of the crystal [22].

Among others, Nagayama et al. and Kim et al. have explored these relations by developing the process with the immersed substrate described in the previous paragraph. The samples produced in these papers were typically polycrystalline with a maximum domain length of tens of micrometers. Nagayama added continuous withdrawal of the substrate at a precise speed, and found that this method could prevent the variations in crystal thickness, and that for example a continuous monolayer could be produced [18].

Kim added further control over the meniscus slope by confining the suspension (by capillary action) between a glass substrate and another, fixed glass slide. The substrate was then raised at a constant speed, while the evaporation rate was controlled by blowing hot air at the drying front. A faster withdrawal rate gave a steeper meniscus, and a thinner crystal. The hot air made it possible to use faster withdrawal rates, thereby shortening production times. Further it was found that, if the concentration was low, and the evaporation rate at the drying front was not sufficiently high, the convective flow of solvent did not bring enough colloids to the contact line to form a continuous layer.

Shape of contact line

Sun et al. turned their attention to the shape of the contact line as the solvent evaporates. A colloidal suspension was inserted between closely spaced glass slides and left to evaporate. They found that in such a cell centimeter-sized single-domain monolayers can be formed, if the contact line is kept straight by capillary action, and the crystal growth can proceed in a constant direction during the evaporation [12]. This is an extraordinary result, especially given the simplicity of the setup.

2.2.2 Self-assembly at an interface

The methods described above rely on the evaporation driven transport of colloidal particles from the bulk of a suspension to the drying front, essentially a three phase contact line, where the assembly takes place. Another

approach is to let the assembly process take place on the surface of a liquid. In the context of this project, a benefit of interfacial assembly is that it more easily, and often exclusively, produces monolayers of colloids.

Ordering mechanisms

The spacial distribution of particles floating on a liquid surface, or partially immersed in a thin liquid film, depends on surface forces in the liquid as well as interparticle forces. It is usually energetically favorable, from a surface energy point of view, to bring the colloids closer to each other. In this case the thermodynamic optimum for a group of spherical particles is a hexagonal close-packed (hcp) lattice [15, 16, 17, 23]. In the process of assembly, once in contact, micrometer-sized or smaller particles will usually adhere to each other by van der Waals interaction. Further reorientation of the lattice is thus hindered. Consequently, purely attractive forces ought to lead to more or less random packing of the particles.

However, colloidal particles are normally at least slightly charged, due to ionization of surface groups. The electrostatic charge provides some interparticle repulsion that allows for increased relative mobility of particles in close proximity to each other, thereby accommodating higher order in formed colloidal crystals. In fact, the surface of colloidal particles is often intentionally functionalized by the addition of sulfonate or carboxyl groups to prevent aggregation of the dispersion.

Langmuir-Blodgett technique

The Langmuir-Blodgett method was developed for assembling dense molecular monolayers by placing the molecules on a liquid surface, the area of which can be contracted in a controlled manner. The molecules are thereby pushed together into a compact, often ordered, monolayer. An instrument called a Langmuir-trough is specifically designed for the method. The layer can then be deposited on a solid substrate by dipping the substrate in the liquid.

Although the method was aimed at molecular monolayers it has also been applied to colloidal monolayers with some success [24, 25, 26]. However, the mechanical contraction of the liquid surface does not seem to be the most effective one for colloids. Once deposited on the liquid surface, other methods can be used to consolidate them.

Related methods applied to colloids

A crucial step in the procedure is the deposition of the colloids onto the surface. They very easily sink and disperse into the bulk of the liquid. When

the liquid used is water, an equal amount of ethanol is often added to the aqueous colloidal suspension, to act as a spreading agent. If the ethanol containing suspension is introduced with proper care on the water surface, it immediately spreads over it. The ethanol then evaporates, and leaves the colloids floating on the surface.

In the method developed by Rybczynski et al. some suspension is applied on the surface of a hydrophilic silicon substrate, and the substrate is slowly brought into contact with a water surface in a petri dish. Once in contact, a Marangoni flow, i.e. a flow driven by the surface tension gradient, will spread the suspension over the water surface and the assembly takes place [27].

A modification to the introduction of the suspension at the interface was developed by Li et al. A piece of hydrophilic glass is placed on the bottom of a petri dish, after which water is poured in to level with the top surface of the glass slide. The suspension is then pipetted onto the piece of glass and spreads to contact the water surface at the edges of it, and is then spread over the water by a Marangoni flow [28]. At this stage, a small quantity of SDS (sodium dodecyl sufate) surfactant solution is added to the surface, which consolidates the monolayer.

From the papers, the role of the surfactant is unclear as to its influence on the ordering of the monolayer. In the paper by Rybczynski, it is assumed that the SDS is responsible for the ordering of a previously unordered monolayer, while others have assumed that previously formed array islands and separate particles are simply pushed together to form a continuous polycrystalline layer [29].

Introduction of dry colloids to liquid surface

Retsch et al. develop a different method of introducing the colloids on a water surface. They spin coat a suspension sparsely onto a hydrophilic substrate, and after drying the colloids are distributed one by one on it. The substrate is then slowly immersed at an incline into the water and the colloids rearrange into a close-packed array at the water contact line [30]. In a variation of this method, the water onto which the colloids are to be deposited is rotated to create a vortex. The suspension is then applied on the moving inclined surface and the vortical movement supposedly assists the assembly process [13].

2.2.3 Self-assembly during spin coating

As mentioned above, spin coating was used to spread colloids sparsely on a substrate. Spin coating can also be used to directly aid self-assembly of

colloids into ordered arrays. In addition to the capillary forces present in a static liquid interface, the shearing forces in the film during spin coating can also induce ordering of the colloids.

Jiang et al. started by spin coating colloids dispersed in a liquid monomer. Depending on the following step, three different structures were produced. By chemically removing the monomer, wafer size polycrystalline colloidal crystals were obtained. Cross linking of the monomer, instead of removal of it, resulted in a solid bi-polymer colloidal crystal. This structure could further be converted into an inverse colloidal crystal, by chemical removal of the colloids [10, 11]. In the method used by Jiang, the liquid monomer is relatively viscous, and the spin times therefore relatively long. Also, to obtain a pure colloidal crystal, the monomer has to be chemically removed.

Mihi et al. instead found that colloidal crystals can be produced by spin coating from a volatile solvent suspension, if the solvent volatility is controlled. Also, importantly to the project at hand, monolayers were produced by the method [31]. A careful study of the dynamics of this crystal formation process was recently published [32].

2.2.4 Methods of choice

Most of the methods described above are relatively simple, but some require special instrumentation like a Langmuir through, or careful control over parameters like temperature and relative humidity. In this project, the simplicity of the methods has been a priority, as well as the potential for creating large pure monolayers on a large scale (centimeter size). These considerations favor the method developed by Rybczynski and modified by Li et al [27, 28]. Also, the evaporative self-assembly in a wedge shaped cell by Sun et al. appears promising [12]. Hence, versions of these methods have been tried in this project. They are here designated *wedge cell assembly* and *assembly by floating*, and are described in the experimental section.

2.3 Electrohydrodynamic Patterning

Both *embedded annealing* and *imprint annealing*, the methods developed in this project, make use of electrohydrodynamic (EHD) annealing. EHD annealing has previously been used to create patterns in originally smooth polymer films. This technique, EHD patterning of polymer films, relies on utilizing the forces that interfaces between media of differing dielectric properties are subject to in an electric field. If the materials separated by the interface are not solid, the forces can rearrange the interface, thus changing

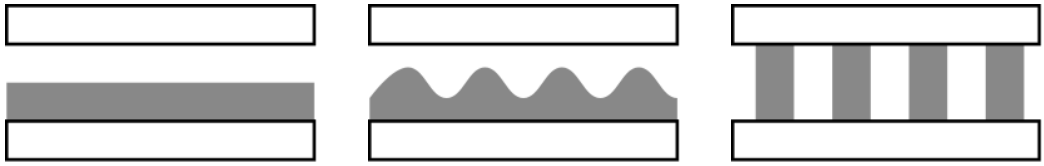

Figure 2.2: A schematic of the basic process of electrohydrodynamic patterning

the morphology of the media.

Schaffer et al. have successfully utilized this effect to create hexagonally arranged pillars on a silicon substrate [33]. The geometry and arrangement of the created pillars is determined by the original film thickness, the spacing of the electrodes and the strength of the electric field. A simple schematic of the patterning process is shown in figure 2.2. An electrode is placed slightly above a polystyrene film spin coated onto another electrode. The film is then annealed above its glass transition temperature (T_g) as a voltage is applied over the electrodes 2.2(a). The electrostatic pressure at the polystyrene-air interface causes an instability in the film 2.2(b), and eventually the film brakes up into columns spanning the gap between the electrodes 2.2(c). As the sample is then cooled before turning the voltage off, the columnar structure of the polymer is conserved.

More complex structures have since then been fabricated by applying the method to multiple layers of polymer and using laterally patterned electrodes [34, 35].

Chapter 3

Experimental

3.1 Wedge cell assembly

The wedge cell experiments resemble the ones presented by Sun et al.[12]. A piece of silicon between two glass slides making up the cell was used as a substrate, instead of the glass slides themselves. Figure 3.1 shows a schematic of the wedge shaped cell. The silicon substrate used was 500 μm thick and about 10×10 mm in size, and the microscope slide glass was 1 mm thick and 26 mm wide. The top slide was cut to roughly appropriate length for the desired geometry. Since the thickness h of the silicon substrate was fixed, the cell angle (the angle between the horizontal substrate and the inclined top slide) could be controlled by varying the distance d between the substrate and the back edge of the bottom slide. Weights (∼25 g each) were placed on the spots indicated by dots in the figure, in order to hold the cell and substrate in place. This was necessary to oppose the capillary forces that would otherwise tend to close the gap between the substrate and the top slide as liquid is injected between them.

A small amount of colloidal suspension (10-15μL) was injected on top of the Si substrate. The suspension was immediately sucked into the space between the top slide and the substrate and formed a contact line with the substrate parallel to the open end of the wedge. The suspension was left to evaporate and as the drying front receded towards the closed end of the cell, colloids were deposited onto the substrate, forming a colloidal crystal. The evaporation rate was controlled by placing the cell inside a container together with an open vessel of water to raise the relative humidity during the experiment. As a container, a large glass petri dish (150 in mm diameter, 20 mm high) with its lid on top, or a plastic 3L box was used. The containers were not perfectly sealed, and holes were cut into the plastic box to allow for

exchange of gases with the surrounding atmosphere. Similarly, the glass petri dish was not perfectly sealed by its lid. The relative humidity was recorded using an integrated circuit humidity sensor (Honeywell HIH-4000-003).

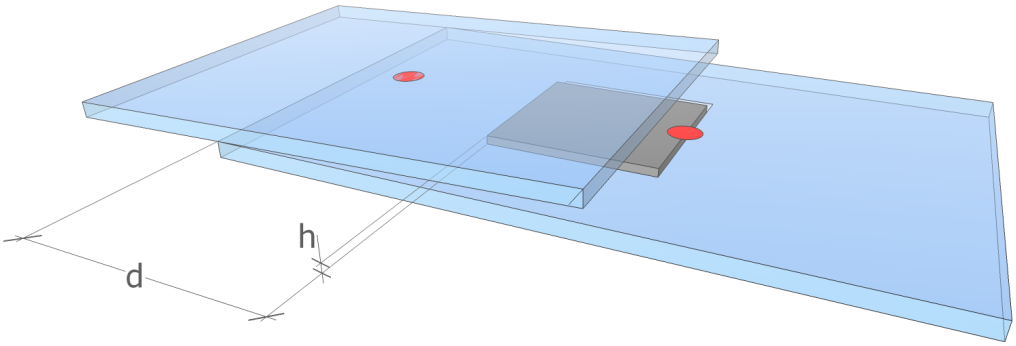

Figure 3.1: A schematic of the wedge shaped cell used for evaporation assisted colloidal self-assembly

3.2 Assembly by floating

The procedure followed to produce two-dimensional colloidal crystals from polymer colloids at an air-water interface is the one described by Rybczynski et al.[27] and further developed by Yu et al [29].

A 1 cm^2 piece of 1 mm thick microscope slide glass was cleaned by sonication for 10 minutes in acetone and isopropanol respectively. The glass piece was then placed at the bottom of an 8 cm in diameter petri dish. Milli-Q water was poured into the petri dish up to slightly above the top surface of the piece of glass. The water surface was pinned to the edges of the glass piece, and did not wet its surface at this point. The subsequent steps are shown in figure 3.2.

A small amount ($\sim 40\mu$L) of aqueous colloidal suspension with 20-50% ethanol added, was pipetted onto the glass piece (3.2(a)). Due to the hydrophilic nature of the glass, the suspension quickly spread to cover the glass.

Once the suspension reached the water contact line it proceeded to flow out on top of the water surface driven by the difference in surface energy

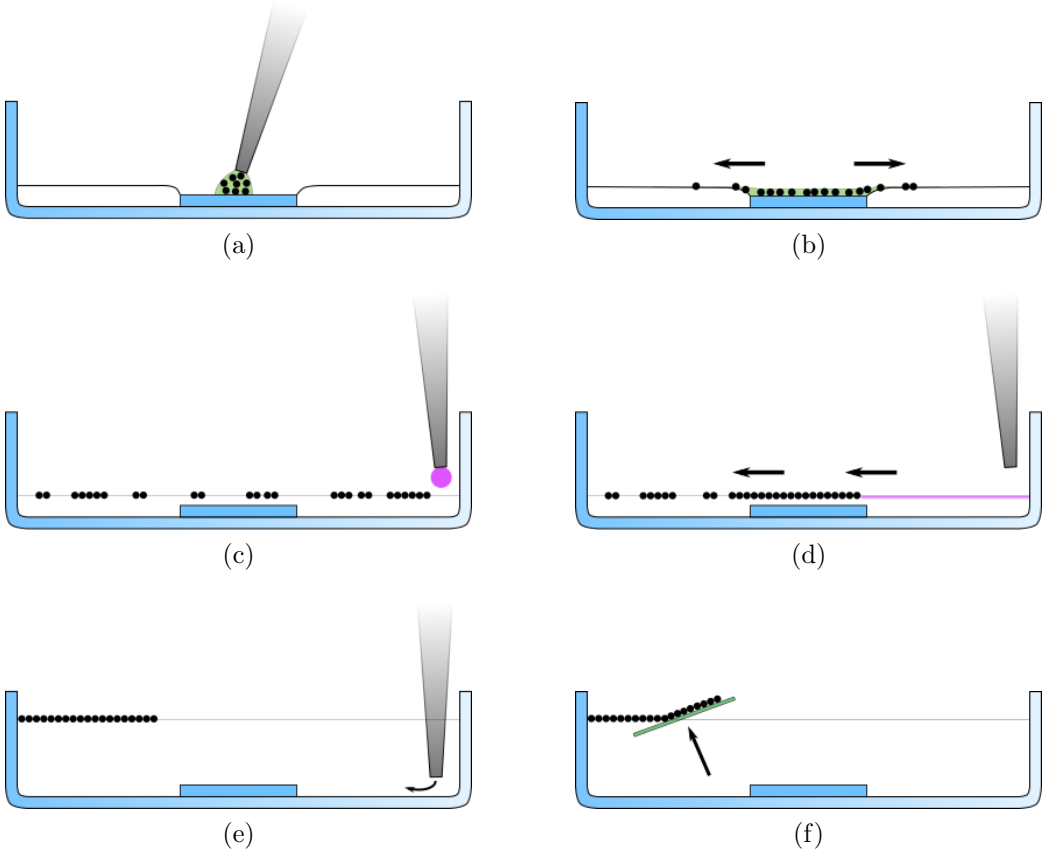

Figure 3.2: A schematic of the process of colloidal assembly by floating

between the ethanol containing suspension and the water in the petri dish (3.2(b)). After a few seconds, all of the suspension had flown out from the glass piece, placing the colloids in a monolayer on the surface of the water. When the glass surface was emptied of suspension the surrounding water flowed in over it, immersing the glass piece. As the residual film of suspension on the glass piece evaporated, some colloids would deposit directly on the surface, but were picked up by the water as it wetted the glass. Colloids could now be seen forming faint features on the water surface. Some colloids also became mixed into the water instead of flowing out on top of it. This mixing seemed to occur at spots on the glass edge that exhibit some roughness, or at the corners of it.

Now, a drop of surfactant was added to the water (3.2(c)). As the surfactant quickly spread over the surface of the water, it pushed the colloids together, into a single connected island (3.2(d)).

More Milli-Q water was then carefully added in the petri dish, so that

the water level was raised (3.2(e)). This was done to facilitate the next step in the procedure, where the colloidal island was picked up on a hydrophilic silicon substrate.

The substrate was cleaned by sonication for 10 min in acetone and isopropanol respectively, followed by 5 min of UV-cleaning to reach the desired hydrophilicity. As shown in figure 3.2(f), the substrate was first immersed into the water, and then slowly lifted up from below the colloidal island at a slight angle ($\sim 10°$).

The colloids can also be deposited on a hydrophobic substrate, by instead pushing it down on the colloids from above, also at a small angle. No systematic experiments were performed using this alternative method.

3.3 Electrohydrodynamic experiments

3.3.1 Experimental set up and materials

A schematic representation of the set up used to anneal both colloids and imprinted features is shown in figure 3.3(a). The annealing is performed in an EHD device inside an oven at ambient atmosphere. Both EHD device electrodes were made of brass. The bottom electrode was a quadratic plate, 0.5 cm thick with 10 cm long sides. The top one was a cube with 2 cm sides. A type K thermocouple was mounted with conducting silver paste (Electrolube silver conductive paint) in a 1 cm deep hole, drilled into the top electrode. Both electrodes were connected to a voltage source using silicone insulated wires. A voltmeter was used to monitor the voltage, and the current was read off the voltage source. To ensure electrical contact and mechanical adhesion during preparations for the experiments, both substrates were mounted on the EHD device electrodes using a small amount of conductive silver paste.

Polystyrene colloids, produced by Polysciences, Inc., were embedded in polydimethylsiloxane (PDMS) in the *embedded annealing*. PDMS was also used as a mold material for thermal imprints. The PDMS was produced by Dow Corning (Sylgard 184, 1 part curing agent mixed into 10 parts base). A thermal nanoimprinter from Obducat was used to imprint polystyrene films for *imprint annealing*. The polystyrene used was produced by Polysciences, Inc (MW=50'000, atactic). SiO_2 colloids, produced by Bangs Laboratories, Inc., were used as spacers in both types of annealing experiments.

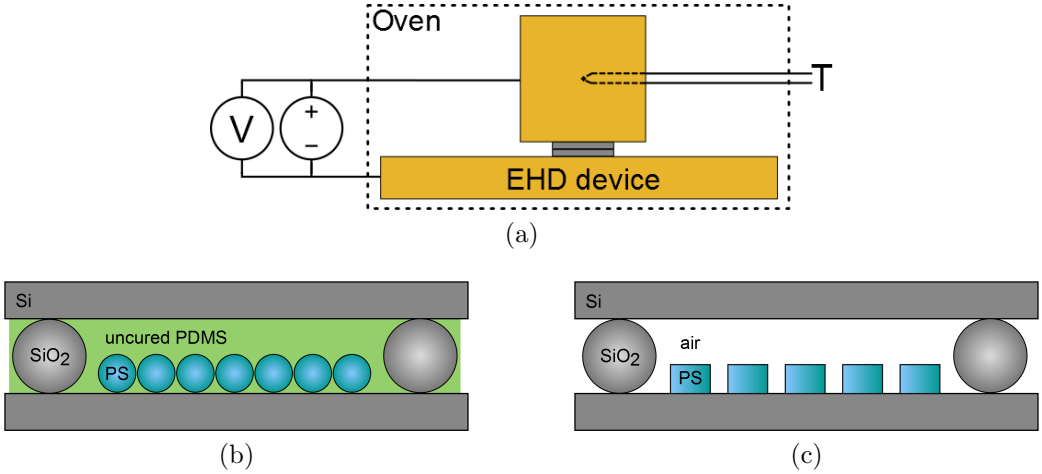

Figure 3.3: A schematic of the set up (a) and sample configurations used to anneal PDMS embedded polystyrene colloids (b) and imprints (c) in electric fields

3.3.2 Embedded annealing

Figure 3.3(b) shows the capacitor configuration used as the starting point of the annealing. Polystyrene colloids were embedded in an uncured PDMS film between silicon substrates. Based on the results of the two self-assembly methods tested, *wedge cell assembly* and *assembly by floating*, a decision was made to use the latter, because it more exclusively produced monolayers. SiO_2 colloids were used to control the spacing of the substrates. The principal idea was to heat the polystyrene colloids to above their glass transition temperature (T_g) to make them soft, and possible to stretch by applying a voltage over the sample. If the colloids would be stretched into pillars, the structure would then be fixed as the PDMS cured.

PDMS films

The PDMS films were prepared as follows: Directly after mixing 10 parts of base with 1 part curing agent, chloroform was added to make a 12 wt% solution that was filtered with an 0.2 µm PTFE filter. Using the PDMS solution a film was spin coated onto a p-doped Si substrate at 2'000 rpm (6'000 rpm/s) for 150 s. After annealing for an hour at 150 °C, the thickness of a PDMS film obtained using this procedure was determined using atomic force microscopy (AFM) to be 1.62 µm.

Annealing procedure

Immediately after the base and the curing agent of the PDMS are mixed, the PDMS starts to cross link. Crucially, any cross linking that happens before the temperature of the sample is above the T_g of polystyrene will counteract the stretching of the colloids in the electric field. Because of this, all of the steps following the mixing of the PDMS need to be conducted with minimum delay. Further, the time it takes for the PDMS to cross link is highly dependent on temperature. According to the product data, the time needed to fully cross link it is 48 h at room temperature, 40 min at 100 °C, 20 min at 125 °C and 10 min at 150 °C. The time the sample spends at elevated heat, but below T_g of the polystyrene, therefore needs to be minimized.

The oven and the bottom electrode of the EHD device inside it are preheated to the desired temperature. The top electrode is also preheated to 60 °C on a hot plate. A monolayer of polystyrene colloids on a p doped Si substrate was prepared. Using a cotton swab dipped in acetone, the edges of the substrate were cleared of polystyrene colloids, and 1.59 µm SiO_2 colloids placed on them to function as spacers. The spacers were transferred with a smooth piece of PDMS from another silicon substrate where they were previously assembled in a monolayer.

On another substrate, a PDMS film was spin coated following the procedure described. To ensure that the polystyrene colloids would be properly embedded in the PDMS film before the annealing, the two substrates were pressed together for 60 s at 5.7 bar at room temperature using the nanoimprinter. The now sandwiched substrates were mounted with silver paste on the preheated top electrode of the EHD device. A drop of silver paste was placed on the free side of the sandwiched samples before the EHD device was asembled inside the oven.

The oven was closed and the voltage turned on. Within one or two minutes, the temperature of the top electrode would rise above 100 °C. The time needed for the sample to equilibrate to the oven temperature depends on the temperature of the oven, but also on any current that may flow though the sample. As a reference point, the time at which the sample reached 100 °C was chosen as the starting time of the annealing. 100 °C is reasonably close to the T_g of polystyrene, and was not passed before closing the oven and turning the voltage on. After the desired time of annealing, the oven was turned off and its door opened to cool the sample. The typical time needed for the sample to cool below 100 °C was about 10 minutes. The voltage was maintained until the temperature of the sample was below 75 °C. For convenience, since the cooling rate of samples differed, the time at which the

oven door was opened was used to define the end of the annealing.

3.3.3 Imprint annealing

Figure 3.3(c) shows the capacitor configuration used as the starting point of the annealing experiments. The idea was to increase the height and decrease the width of imprinted features by stretching them in an electric field. In order to make the polystyrene malleable it was heated to above T_g. When cooled, the transformation of the features was fixed.

Control of polystyrene film thickness

Polystyrene solutions in toluene were prepared in new glass vials (rinsed with toluene and blown dry in a nitrogen stream) and filtered using an 0.2 µm PTFE filter. The dependence of polystyrene film thickness on spin speed and solution concentration was determined by spin coating films from a number of solutions at different speeds on clean silicon substrates. The films were then scratched using a scalpel and the film thickness was measured by AFM. An approximately 10×10 µm AFM image was captured in the center of each sample, and the thickness of the film was determined from an average on each image. The results are presented in figure 3.4.

Improved dewetting by surface functionalization

For the imprinted features to grow significantly in height, the polystyrene has to partially dewet the substrate. That is, the contact area of each feature with the silicon substrate decreases during annealing. To facilitate this process, hexamethyldisilazane (HMDS) treatment was used in some samples to alter the surface energy between the substrate and the polystyrene. The treatment was carried out by HMDS vapor exposure.

The substrates were placed in a holder inside a sealed beaker. A small amount of HMDS was put in the beaker, below the substrate holder. The beaker was heated from below on a hot plate kept at 85 °C for three hours, while being cooled from above by an ice bath placed on top of the beaker lid. After the treatment, the substrates were sonicated for 20 minutes in acetone and isopropanol respectively.

As intended, the HMDS treatment resulted in decreased adhesion between the polystyrene and the substrate, which was manifested in different ways. Imprinting of the films was no longer possible using ETFE molds, because the polystyrene would stick to the mold when it was lifted off the substrate. Imprinting with PDMS molds was still possible as the polystyrene did not stick

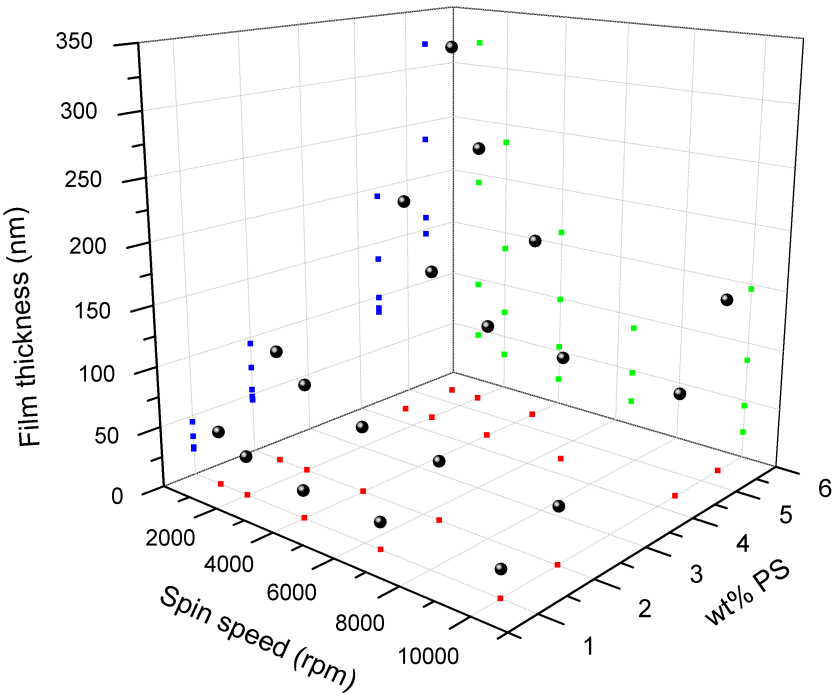

Figure 3.4: Spin speed- and concentration dependence of film thickness for polystyrene in toluene

to them. It was also clear that the polystyrene films on the HMDS treated substrates were less stable at elevated temperatures. This was observed during imprinting. On the edges of the substrate where the polystyrene film was not covered by the mold, the film would spontaneously dewet the surface, forming small drops. When imprinting films on untreated substrates, the film stayed smooth outside of the imprinted region. An adverse side effect of the HMDS treatment was apparent in the film preparation. During spin coating on an HMDS treated substrate, the polystyrene solution would often be ejected completely off the substrate.

Imprinting procedure

All silicon substrates used were cut to approximately 1.5×1.5 cm pieces and ultrasonicated for 10 min in acetone and isopropanol respectively. The polystyrene imprints on the bottom substrates were produced by thermally imprinting spin coated films using ETFE and PDMS molds. Films were spin

coated following the procedure described above and imprinted for 300 s at 150 °C and 20 bar. The residual layer between the imprinted features was minimized by making sure that the films used were not thicker than to completely fill the holes in the mold. By using even thinner films, the height of the resulting imprints could then be varied.

Experiments were conducted using two different mold sizes, an ETFE mold with a square pattern of 0.8 µm deep 4 µm wide holes with a spacing of 12 µm, and a PDMS mold with a square pattern of truncated square 0.4 µm deep pyramidal holes with a base width of 1.4 µm and a spacing of 1.9 µm. AFM images and profiles of the molds are shown in figure 3.5. Not shown is a PDMS mold of the same size as the ETFE mold, that was used for some of the samples.

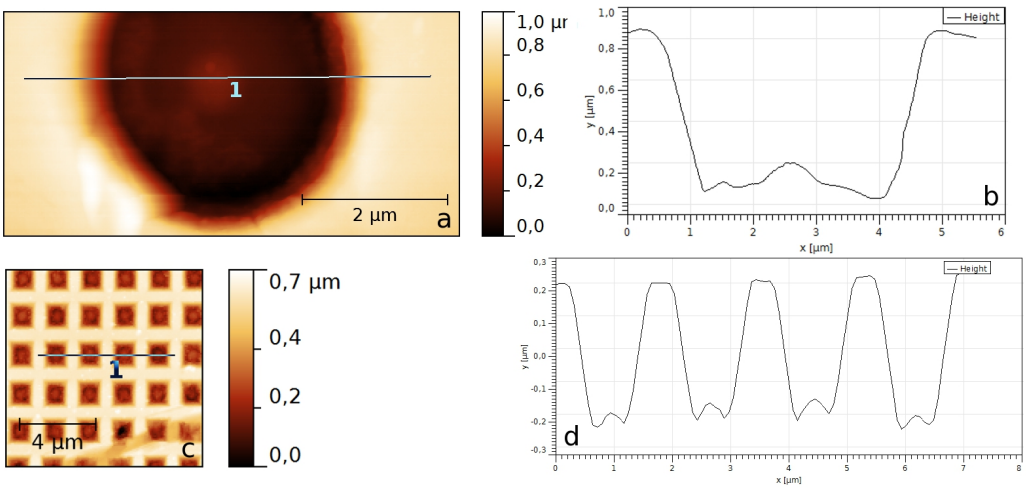

Figure 3.5: AFM images and height profiles of molds used to make polystyrene imprints. ETFE mold shown in a and b, PDMS mold in c and d

Annealing procedure

$1 - 2$ µL of 1.59 µm SiO_2 colloidal suspension was placed on the top electrode. It was prepared by mixing 1 part (by volume) of 10.27 wt% aqueous suspension in 1000 parts ethanol. The suspension readily spread to cover the substrate, and as the ethanol evaporated, spacers were sparsely distributed over the surface.

The oven was preheated to the desired temperature. For annealing times shorter than 4 hours, the bottom electrode was also preheated in the oven. Both substrates were then mounted to the electrodes using a drop of silver

paste, and the set up was assembled inside the oven. The oven was then closed, and the voltage source turned on. As in *embedded annealing*, the reported annealing time of the experiments was measured from when the sample temperature reached 100 °C to the start of cooling by turning off the oven and opening the oven door. The voltage was maintained until the temperature of the sample was below 75 °C.

3.4 Characterization

The colloidal self-assembly techniques were characterized mainly by optical microscopy. The electrohydrodynamic experiments on imprinted features were characterized by optical microscopy and AFM, using CT130 and CT300 tipolystyrene from Nanoscience Instruments on a Veeco Multimode AFM. The electrohydrodynamic experiments on embedded colloids were mainly characterized by SEM using two different instruments, a Cambridge Stereoscan 360 iXP and Philips ESEM XL30. Additional characterization was made by AFM. Optical microscopy was also used in setting up the experiments, to make sure that substrates and films were clean before starting the annealing.

Chapter 4

Results

4.1 Wedge cell assembly

Figure 4.1 shows a microscope image of 0.75 μm polystyrene colloids assembled on a silicon substrate using the wedge cell method. The light gray areas were determined by higher magnification microscopy to correspond to hexagonally close-packed monolayer areas. The figure also shows how, at this magnification, the areas of more sparsely distributed colloids appear pink, and areas covered by more than one layer appear darker, beginning with green for double layers. The lightest, almost white areas are where the silicon substrate is uncovered.

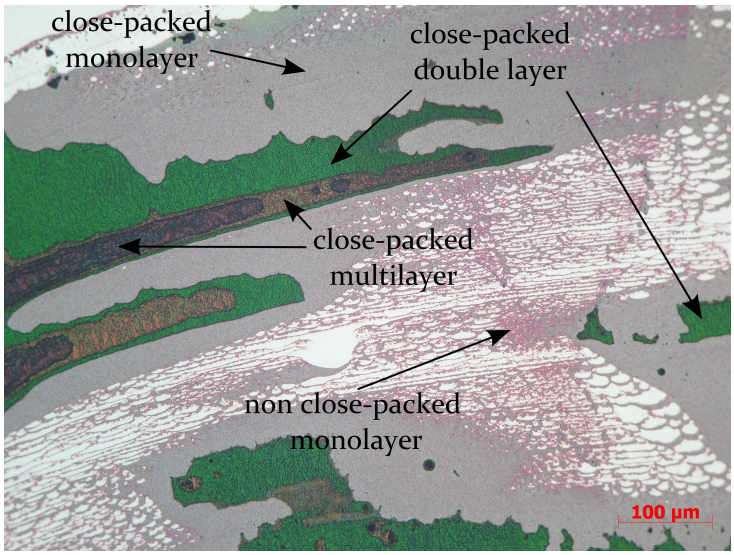

Figure 4.1: 0.75 μm colloids assembled in a wedge cell on a silicon substrate

Using the wedge cell method, close packed colloidal crystals of both polystyrene and SiO_2 colloids were produced. Figure 4.2 shows monolayers of 0.75 μm polystyrene colloids and 1.59 μm and 3 μm SiO_2 colloids. The individual colloids can easily be seen in 4.2(c), and even though it is hard to make out individual colloids in (a) and (b), the domain edges and impurities in the ordered monolayer can be seen as a dark network of lines. The increase in order with increasing colloid size apparent in the images is representative of the experiments.

Table 4.1 shows stitched together microscope images of a number of samples arranged by the cell angle and relative humidity used for each sample. Each stitched image covers an area about 5 mm long, along the center of the sample. The evaporation, and thus the deposition of colloids, has started from the left. Most of the colloids were deposited at the beginning of the process, with the coverage decreasing towards the end of the experiment. Figure 4.1 shows an image taken with the same objective as all images in table 4.1, and can be used to determine the number of layers of colloids. Judging from these experiments, the area covered by a monolayer tends to increase with increasing relative humidity and decreasing cell angle, but with the cost of similarly increasing multilayers.

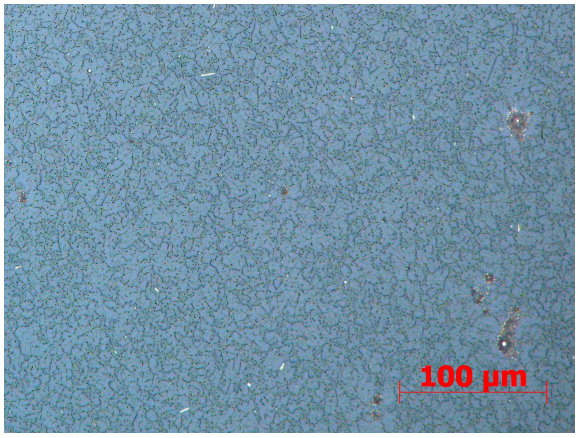

(a)

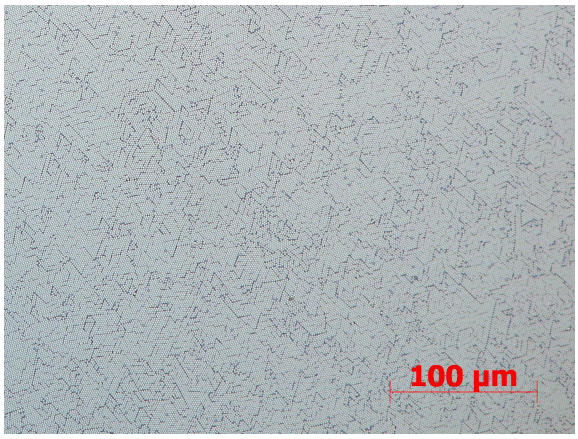

(b)

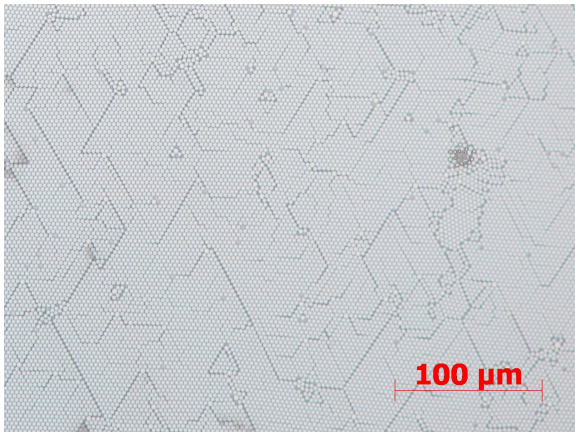

(c)

Figure 4.2: Monolayers produced with the wedge cell method. (a), (b) and (c) show 0.75 µm polystyrene colloids, 1.59 µm SiO_2 colloids and 3 µm SiO_2 colloids respectively

Table 4.1: Optical micrographs of wedge cell assembly experiments with 0.75 μm colloids, all from 0.5 wt % suspensions. Cell angle on the horozontal axis, relative humidity on the vertical

	1°	2°	2.9°
88%		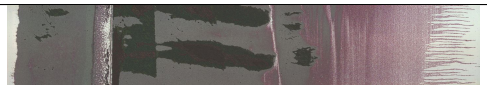	
76%	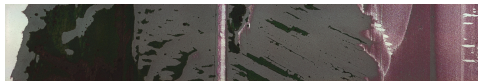	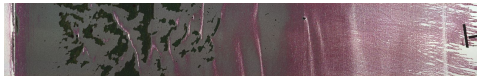	
48%	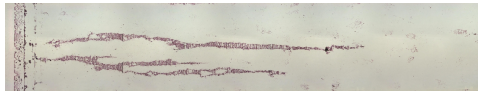		
8.8%			

4.2 Self-assembly by floating

Colloidal crystals of 1 and 0.75 μm polystyrene colloids were produced using *assembly by floating*, as described in section 3.2. Figure 4.3 shows microscope images of hexagonally close-packed 1 μm colloids and an AFM image of hexagonally close packed 0.75 μm colloids, both picked up on Si substrates. What looks like a sharp edge in the upper right corner of each colloid is an artifact from a dirty or damaged AFM tip. The produced samples showed a very broad distribution of domain sizes, with the largest ones, comprised of 1 μm colloids, being up to 46'000 μm^2 in area.

The floating method almost exclusively produced monolayers, as opposed to multilayers, but imperfections in the form of separate colloids on top of the monolayer were still present. These can be seen as blurry dots in 4.3(a) and 4.3(b). They appear blurry since they lie above the focal plane. The overlaying colloids are believed to originate from the colloids that were unintentionally mixed into the water in the petri dish instead of staying afloat.

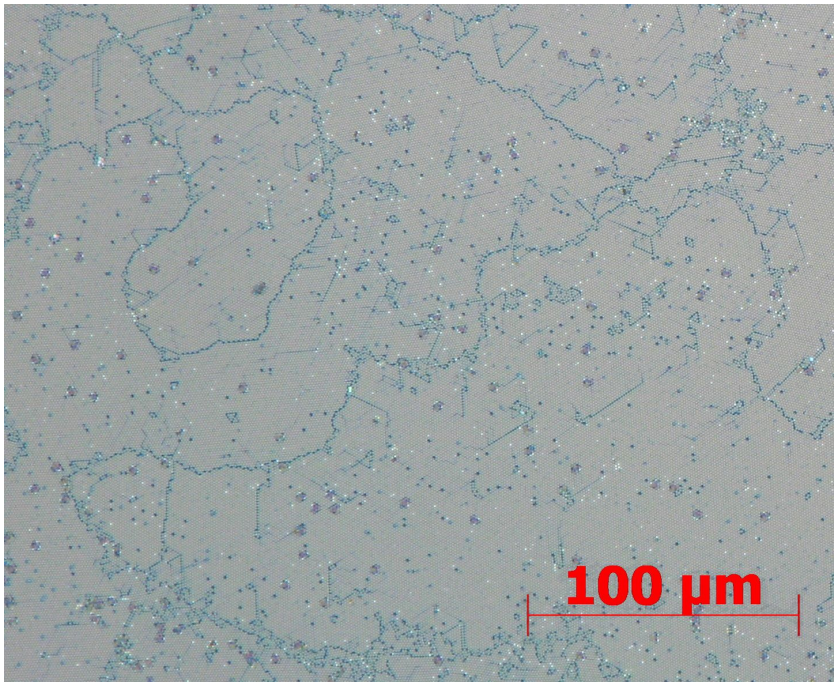

(a)

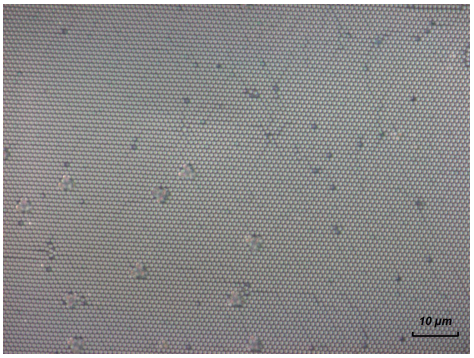

(b)

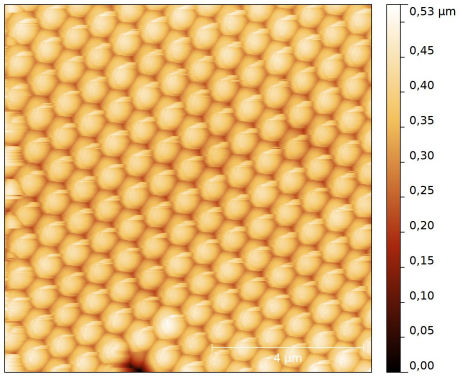

(c)

Figure 4.3: Monolayers produced with the floating method. (a) and (b) are optical micrographs at different magnifications of 1 µm polystyrene colloids. (c) is an AFM image of a monolayer of 1.75 µm colloids

4.3 Embedded annealing

The temperatures and voltages used to anneal the samples are shown in table 4.2. All of the samples were annealed long enough to completely cross link the PDMS at the specific temperature used. Two samples were annealed at

115 °C and 50 V. The PDMS film on these samples was too thin (∼1.4 μm) to completely fill the gap, defined by the spacers, between the substrates. Because of this air gap it was possible to separate the substrates and characterize them using AFM. When separating the substrates, the PDMS film broke differently in different regions of the sample. Either it broke off cleanly at one of the silicon surfaces, leaving all of it on the adjacent substrate, or it broke at either side of the colloidal layer.

Figure 4.4 shows an AFM scan of the top substrate (on which the PDMS film was originally spin coated) in a region where the whole film, including colloids, was left on it. The hexagonal arrangement of holes seem to be where the colloids have sunken into the PDMS film. The holes indicate that the PDMS could not flow all the way in under the colloids, but their small diameter shows that the colloids are almost completely embedded in the film. As the PDMS films in the rest of the annealed samples were thick enough to completely fill the gap, the substrates were practically glued together after annealing. Because of this, the sandwiched substrates were freeze fractured together, so that SEM could be performed on the cross section of the film between the substrates. None of the samples showed any stretching of the colloids. Figure 4.5 shows SEM images of two different samples in which the colloids are seen inside the PDMS film.

Table 4.2: Conditions used for annealing PDMS embedded PS colloids in an electric field

Temperature [°C]	Voltage [V]
115	50
115	50
120	50
120	100
120	150
120	200
140	50
140	100
140	150
140	200

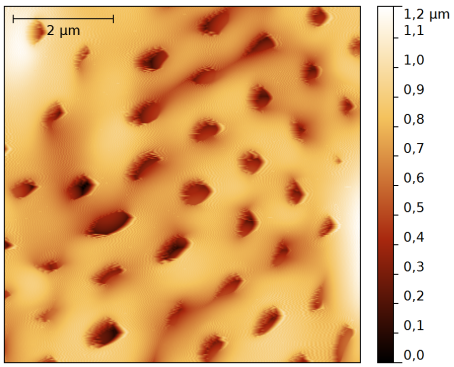

Figure 4.4: AFM scan normal to the PDMS film surface in an annealed sample.

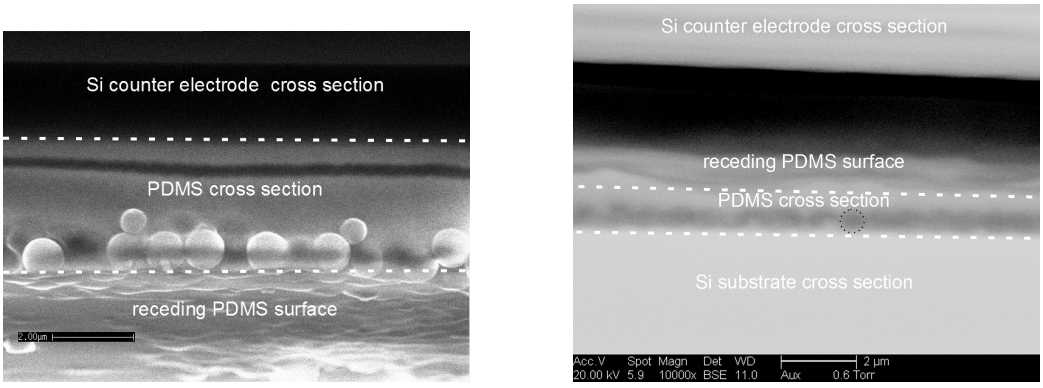

(a) (b)

Figure 4.5: SEM images of PDMS embedded colloids after annealing. (a) shows a secondary electron scan of a sample annealed at 115 °C and 50 V, and (b) shows a back-scattering electron image of a sample annealed at 140 °C and 200 V. For clarity, one of the colloids has been circled with a dotted line.

4.4 Imprint annealing

All of the experiments were conducted at 50 V with 1.59 μm spacers. The annealing times varied from 1 to 64 h. Appendix A contains a list of experimental conditions for all imprint annealing experiments. The stretching effect of the field during annealing is well illustrated by the optical micrograph in figure 4.6. An abrupt transition from growing and fully developed pillars to coalescing ones is seen where the top electrode ended.

Figure 4.7 summarizes measured pillar diameters of fully developed pillars, i.e. pillars that spanned the gap after the annealing. Each point is an average of 10 pillars measured using optical microscopy in one region of one sample. The pillar volumes for each point were determined from measurement of the unit area of the imprint in that region, and the original film thickness of the sample in question. For a given gap height, the diameter is expected to scale as the square root of the volume, and the data fits this prediction reasonably well. Figure 4.8 shows optical micrographs of a sample, focused at the base and at the top of the pillars respectively. It is clear from this figure that the pillars are slightly wider at the base than at the top. Usually the pillars were broken somewhere in the middle, instead of at one of the substrates.

By comparing the top and base diameter of a number of samples, an approximate relationship between the top and base diameter of a pillar was determined. Using this mean diameter and the known volume, the height of the pillars were approximated. These are shown in figure 4.9. The horizontal line indicates the spacer height. The validity of the approximated heights for the pillars is supported by the fast that the heights below the spacer height are from samples where broken spacers could be observed after annealing. Most of the heights are bigger than the spacers. This is not very surprising, as it is very challenging to keep the substrates clear of particles bigger than the spacers in a non-cleanroom environment. Using the approximated mean diameters and heights, the aspect rations of the pillars were also calculated and are shown in figure 4.10.

Another detailed wiew of the effect of the annealing is shown in the optical images and AFM profiles of a sample with 6 μm^3 pillar volume shown in figure 4.11. The optical micrographs and the AFM profiles are images of exactly the same area and pillar, before and after annealing.

In the experiments, films down to 20 nm were used, and in a number of samples, it was evident that the pillars did span the gap, but that most seemed to have broken off when molten, forming drops on both substrates after cooling. The cause of this was not determined, though longer cooling times seemed to alleviate this problem.

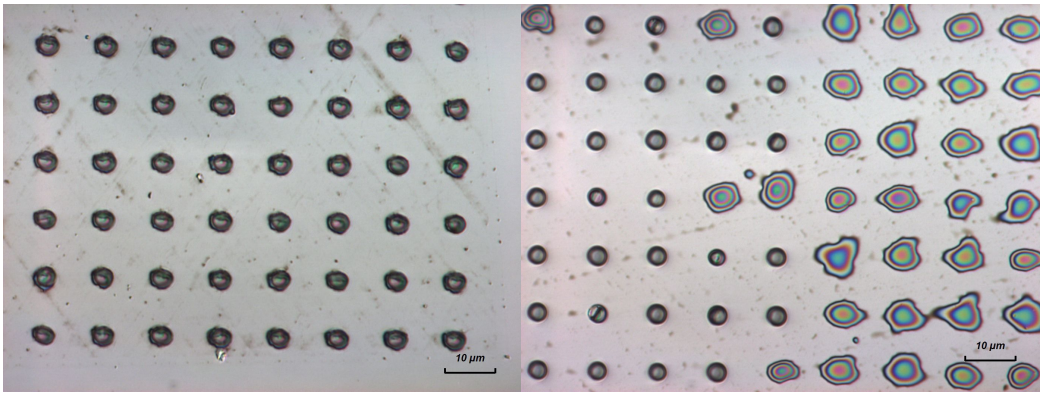

(a) (b)

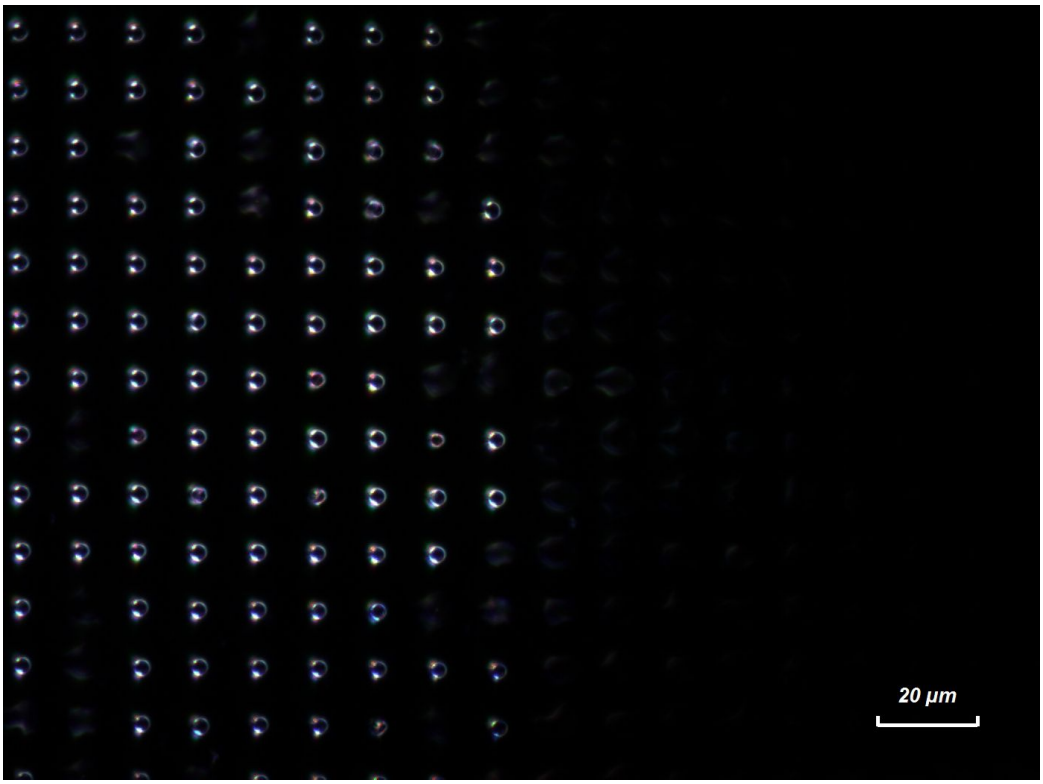

(c)

Figure 4.6: Optical micrographs of a sample annealed at 140 °C and 50 V for 25 minutes. (a) shows the sample before annealing, (b) after annealing. (c) shows the same region in dark field mode. In (b) and (c), a clear vertical line corresponding to the position of the edge of the counter electrode can be seen.

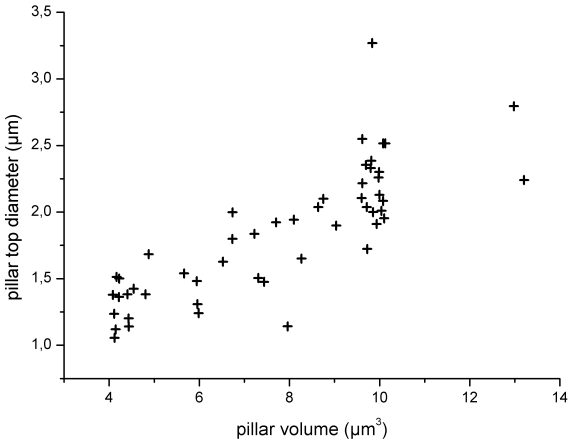

Figure 4.7: Measured diameters of fully developed pillars after annealing

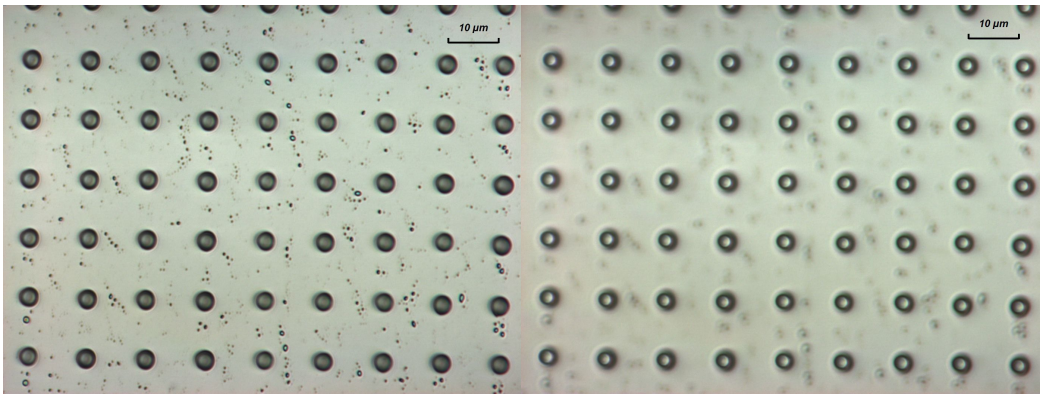

(a) (b)

Figure 4.8: Optical micrographs of a sample from a 70 nm film annealed for 17 hours at 50 V and 140°C. (a) and (b) are focused on the base and top of the pillars respectively

None of the experiments using the 1.9 µm PDMS mold produced pillars spanning the gap. Figure 4.12 shows an AFM profile of an imprinted sample prior to annealing. An optical micrograph of a sample prior to imprinting, and one of the best annealing results so using the small mold are shown in figure 4.13.

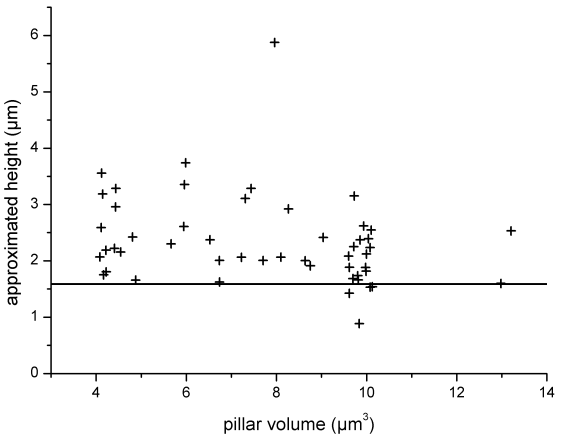

Figure 4.9: Calculated heights of fully developed pillars after annealing

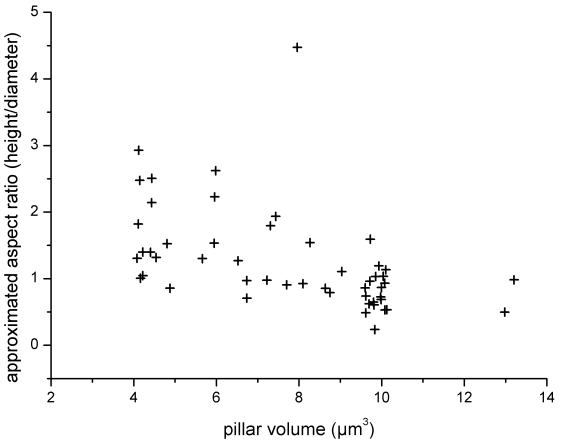

Figure 4.10: Calculated aspect ratios of fully developed pillars after annealing

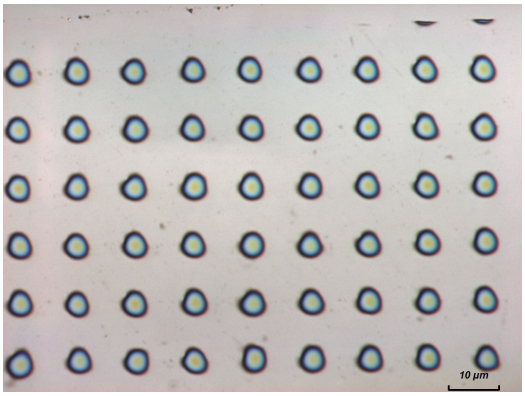

(a)

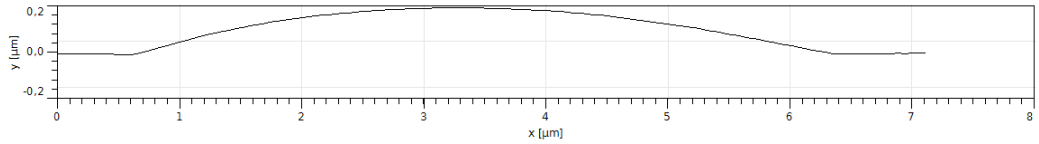

(b)

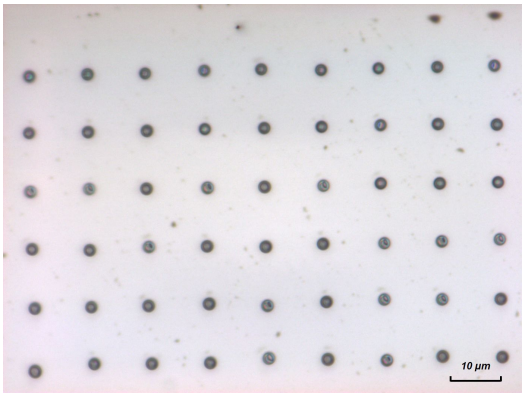

(c)

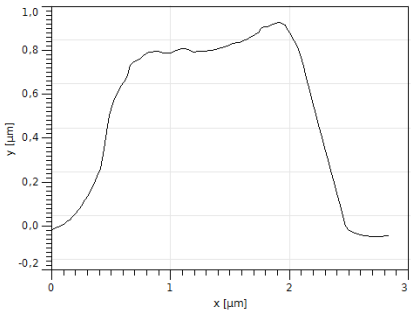

(d)

Figure 4.11: Optical micrographs and AFM profiles of the same spot and pillar on EHD43 before ((a) and (b)) and after annealing ((c) and (d))

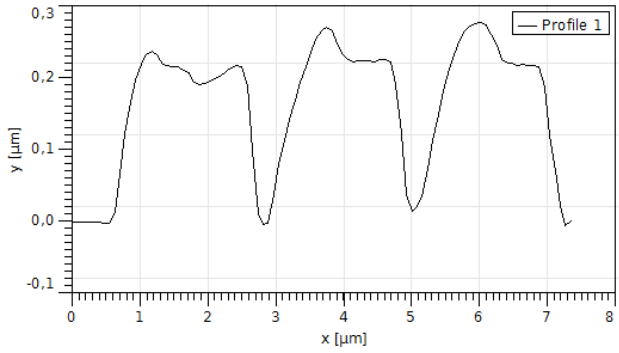

Figure 4.12: An AFM profile of a sample imprinted with the 1.9 µm hole mold prior to annealing

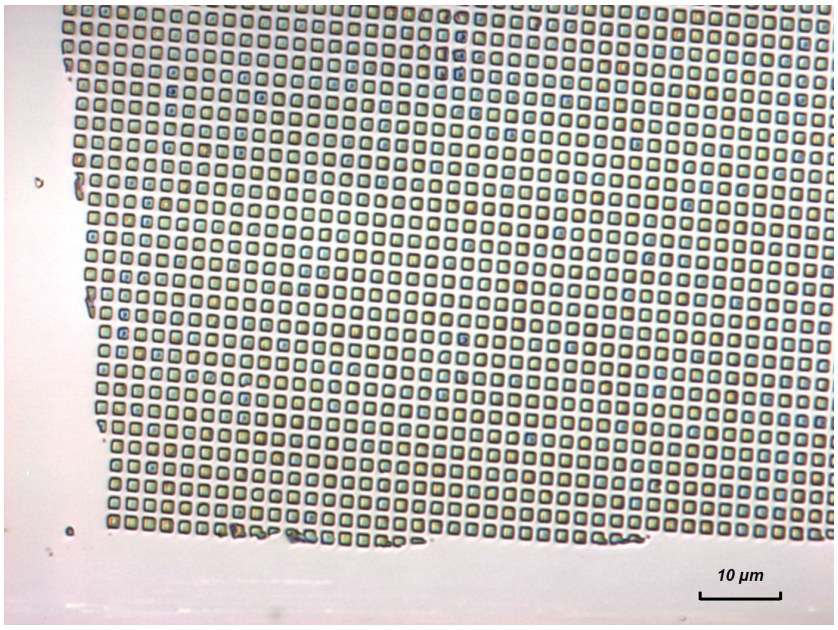

(a)

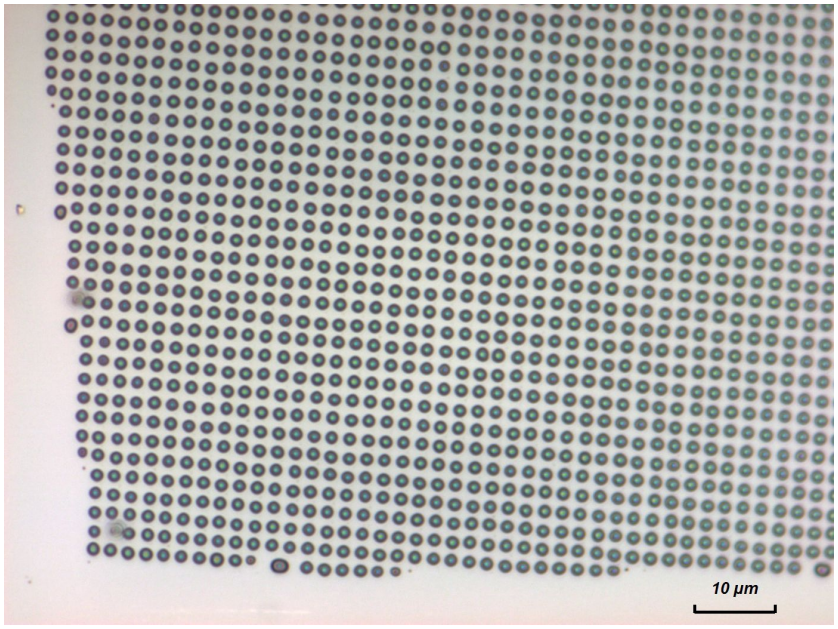

(b)

Figure 4.13: Sample with 1.9 µm features before (a) and after annealing at 190 °C and 50 V for 15 hours (b). HMDS treated before spin coating.

Chapter 5

Conclusion

In this work, I have shown shown that electrohydrodynamic annealing can be used to increase the aspect ratio of thermoplastic polymer structures such as thermally imprinted polystyrene features. The periodicity of the imprinted features was conserved in the process, while the resulting features are columnar in shape, irregardless of the shape of the original feature. Figure 4.10 shows promise for further increased aspect ratios, and the limits of the process should be determined. This method, applied to the production of organic solar cells, shows potential of producing geometries well suited for efficient charge separation. However, the method should be applied to significantly smaller original imprints to get closer to the typical diffusion length of excitons as described in Chapter 1

Comparison of the results of the experiments done with the different size molds suggest that the process might be limited not by the original height, but by the volume available for the pillar to form from. Especially, figures 4.11(b) and 4.12 seem to suggest this to be the case, since the feature imprinted with the larger mold is initially lower in height that the one imprinted with the smaller mold. In spite of this, the initially lower features spanned the gap in a mere 4 hours, while annealing for as long as 65 hours using the smaller mold has not produced pillars spanning the gap. It is suggested that this eventual limitation should be further investigated.

Annealing of PDMS embedded colloids in an electric field, aiming to stretch the colloids into pillars, did not produce positive results. This is assumed originate from the PDMS cross-linking before stretching of the colloids takes place at the annealing temperatures used. A suggestion for future experiments could be to embed the polystyrene colloids in only a PDMS base, leaving out the curing agent. This could also alleviate the characterization of the colloids after annealing, since the substrates should not adhere to each other.

References

[1] PM Vitousek. Beyond global warming - ecology and global change. *Ecology*, 75(7):1861–1876, October 1994.

[2] RW Bentley. Global oil & gas depletion: an overview. *Energy Policy*, 30(3):189–205, February 2002.

[3] K Jakobsson, B Soderbergh, M Hook, and K Aleklett. How reasonable are oil production scenarios from public agencies? *Energy Policy*, 37(11):4809–4818, November 2009.

[4] SE Shaheen, DS Ginley, and GE Jabbour. Organic-based photovoltaics. toward low-cost power generation. *MRS Bulletin*, 30(1):10–19, January 2005.

[5] SE Gledhill, B Scott, and BA Gregg. Organic and nano-structured composite photovoltaics: An overview. *Journal of Materials Research*, 20(12):3167–3179, December 2005.

[6] JD Joannopoulos, PR Villeneuve, and S Fan. Photonic crystals. *Solid State Communications*, 102(2-3):165–173, April 1997.

[7] W Stober. Controlled growth of monodisperse silica spheres in the micron size range. *Journal of Colloid and Interface Science*, 26(1):62–69, January 1968.

[8] Public domain, Java-based, scientific image processing program. rsb.info.nih.gov/ij/.

[9] P Jiang, JF Bertone, KS Hwang, and VL Colvin. Single-Crystal colloidal multilayers of controlled thickness. *Chemistry of Materials*, 11(8):2132–2140, 1999.

[10] P Jiang and M McFarland. Large-Scale fabrication of Wafer-Size colloidal crystals, macroporous polymers and nanocomposites by Spin-Coating. *Journal of the American Chemical Society*, 126(42):13778–13786, October 2004.

[11] P Jiang, T Prasad, M McFarland, and V Colvin. Two-dimensional nonclose-packed colloidal crystals formed by spincoating. *Applied Physics Letters*, 89(1):011908, 2006.

[12] J Sun, C Tang, P Zhan, Z Han, Z Cao, and Z Wang. Fabrication of Centimeter-Sized Single-Domain Two-Dimensional colloidal crystals in a Wedge-Shaped cell under capillary forces. *Langmuir*, 26(11):7859–7864, June 2010.

[13] F Pan, J Zhang, C Cai, and T Wang. Rapid fabrication of Large-Area colloidal crystal monolayers by a vortical surface method. *Langmuir*, 22(17):7101–7104, 2006.

[14] RD Deegan, O Bakajin, TF Dupont, G Huber, SR Nagel, and TA Witten. Capillary flow as the cause of ring stains from dried liquid drops. *Nature*, 389(6653):827–829, October 1997.

[15] N Denkov, O Velev, P Kralchevski, I Ivanov, H Yoshimura, and K Nagayama. Mechanism of formation of two-dimensional crystals from latex particles on substrates. *Langmuir*, 8(12):3183–3190, December 1992.

[16] K Nagayama. Two-dimensional self-assembly of colloids in thin liquid films. *Colloids and Surfaces A: Physicochemical and Engineering Aspects*, 109:363–374, April 1996.

[17] ND Denkov, PA Kralchevsky, and IB Ivanov. Lateral capillary forces and Two-Dimensional arrays of colloid particles and protein molecules. *Journal of Dispersion Science and Technology*, 18(6):577–591, 1997.

[18] AS Dimitrov and K Nagayama. Continuous convective assembling of fine particles into Two-Dimensional arrays on solid surfaces. *Langmuir*, 12(5):1303–1311, January 1996.

[19] R Micheletto, H Fukuda, and M Ohtsu. A simple method for the production of a Two-Dimensional, ordered array of small latex particles. *Langmuir*, 11(9):3333–3336, 1995.

[20] G Lozano and H Míguez. Relation between growth dynamics and the spatial distribution of intrinsic defects in self-assembled colloidal crystal films. *Applied Physics Letters*, 92(9):091904, 2008.

[21] G Lozano and H Míguez. Growth dynamics of Self-Assembled colloidal crystal thin films. *Langmuir*, 23(20):9933–9938, 2007.

[22] MH Kim, SH Im, and OO Park. Rapid fabrication of two- and Three-Dimensional colloidal crystal films via confined convective assembly. *Advanced Functional Materials*, 15(8):1329–1335, August 2005.

[23] GS Lazarov, ND Denkov, OD Velev, PA Kralchevsky, and K Nagayama. Formation of two-dimensional structures from colloidal particles on fluorinated oil substrate. *Journal of the Chemical Society, Faraday Transactions*, 90(14):2077, 1994.

[24] B van Duffel, RHA Ras, FC De Schryver, and RA Schoonheydt. Langmuir-Blodgett deposition and optical diffraction of two-dimensional opal. *J. Mater. Chem.*, 11(12):3333–3336, 2001.

[25] S Reculusa and S Ravaine. Synthesis of colloidal crystals of controllable thickness through the LangmuirBlodgett technique. *Chemistry of Materials*, 15(2):598–605, January 2003.

[26] M Bardosova, M Pemble, I Povey, and R Tredgold. The Langmuir-Blodgett approach to making colloidal photonic crystals from silica spheres. *Adv. Mater.*, 22(29):3104–3124, 2010.

[27] J Rybczynski. Large-scale, 2D arrays of magnetic nanoparticles. *Colloids and Surfaces A: Physicochemical and Engineering Aspects*, 219(1-3):1–6, June 2003.

[28] C Li, G Hong, P Wang, D Yu, and L Qi. Wet chemical approaches to patterned arrays of Well-Aligned ZnO nanopillars assisted by monolayer colloidal crystals. *Chemistry of Materials*, 21(5):891–897, March 2009.

[29] Jie Yu, Qingfeng Yan, and Dezhong Shen. Co-Self-Assembly of binary colloidal crystals at the AirWater interface. *ACS Applied Materials & Interfaces*, 2(7):1922–1926, July 2010.

[30] M Retsch, Z Zhou, S Rivera, M Kappl, XS Zhao, U Jonas, and Q Li. Fabrication of Large-Area, transferable colloidal monolayers utilizing Self-Assembly at the Air/Water interface. *Macromol. Chem. Phys.*, 210(3-4):230–241, 2009.

[31] A Mihi, M Ocaña, and H Míguez. Oriented Colloidal-Crystal thin films by Spin-Coating microspheres dispersed in volatile media. *Adv. Mater.*, 18(17):2244–2249, 2006.

[32] M Giuliani, W González-Viñas, K Poduska, and A Yethiraj. Dynamics of crystal structure formation in Spin-Coated colloidal films. *The Journal of Physical Chemistry Letters*, 1(9):1481–1486, May 2010.

[33] E Schaffer, T Thurn-Albrecht, T Russell, and U Steiner. Electrically induced structure formation and pattern transfer. *Nature*, 403(6772):874–877, February 2000.

[34] MD Dickey, S Gupta, KA Leach, E Collister, CG Willson, and TP Russell. Novel 3-D structures in polymer films by coupling external and internal fields. *Langmuir*, 22(9):4315–4318, 2006.

[35] KA Leach, S Gupta, MD Dickey, CG Willson, and TP Russell. Electric field and dewetting induced hierarchical structure formation in polymer/polymer/air trilayers. *Chaos: An Interdisciplinary Journal of Nonlinear Science*, 15:047506, 2005.

Appendix A

Conditions for imprint annealing experiments

Table A.1, A.2 and A.3 summarize the experimental conditions and results of electrohydrodynamic experiments done on imprints made using the molds with 4 μm diameter holes. The originally imprinted pillar heights reported are based on the assumption of perfect cylinders 4 μm in diameter made up of the volume of polystyrene per unit cell of the mold.

Table A.4 summarizes the annealing experiments done on polystyrene imprints made using the PDMS mold with 1.9 μm pyramidal holes.

Table A.1: Experimental conditions and comments for annealed samples imprinted using molds with 4 μm diameter holes, continued in table A.2. Fully developed pillars have been measured for the plots on samples marked *

sample ID	substrate treatment before spin coating	mold	PS film thickness [nm]	imprinted pillar height [nm]	counter electrode treatment	temperature [°C]	annealing time [hh:mm]	comments
EHD41*	sonication 5 min in acetone and IPA	ETFE	73,4	841	sonication 5 min in acetone and IPA	140	00:25	Fully developed pillars.
EHD30							00:40	Some increase in height of pillars as evident from decrease in base diameter.
EHD31*							01:00	Fully developed pillars.
EHD42							02:00	Not much growth, No coalescence.
EHD40							16:16	No growth, some coalescence.
EHD37					sonication 5 min in acetone and IPA. HMDS treated for 3 h		01:19	No growth, some coalescence.
EHD36							14:37	No growth, no coalescence.
EHD34*							16:53	Fully developed pillars
EHD35*							19:20	Fully developed pillars
EHD46						190	01:04	No growth, No coalescence.
EHD32	sonication 5 min in acetone and IPA	ETFE	54	619	sonication 5 min in acetone and IPA	140	01:00	No growth, No coalescence.
EHD39*	sonication 5 min in acetone and IPA	ETFE	45,2	516	sonication 5 min in acetone and IPA. HMDS treated for 3 h	175	04:00	Some fully developed pillars.
EHD68						190		Imprint destroyed. Substrates rotated during annealing.
EHD43*					sonication 5 min in acetone and IPA.		04:00	Fully developed pillars.
EHD59	sonication 5 min in acetone and IPA	ETFE	32,2	369	sonication 5 min in acetone and IPA.		17:33	Very few fully developed pillars
EHD60							22:00	Very few pillars fully developed. Most more or less unaffected.
EHD61		PDMS					39:30	Pillars have spanned the gap. Most seem to have broken when molten.
EHD62							65:00	Pillars have spanned the gap. Most seem to have broken when molten.
EHD63							15:00	Pillars have spanned the gap. Most seem to have broken when molten.

Table A.2: Experimental conditions and comments for annealed samples imprinted using molds with 4 µm diameter holes, continued from table A.1. Fully developed pillars have been measured for the plots on samples marked *

sample ID	substrate treatment before spin coating	mold	PS film thickness [nm]	imprinted pillar height [nm]	counter electrode treatment	temperature [°C]	annealing time [hh:mm]	comments
EHD38	sonication 5 min in acetone and IPA	ETFE	21,5	246	sonication 5 min in acetone and IPA. HMDS treated for 3 h	140	14:53	No growth, No coalescence.
EHD56					sonication 5 min in acetone and IPA.	190	01:00	Some growth, but not much.
EHD47					sonication 5 min in acetone and IPA. HMDS treated for 3 h		01:30	Short circuit. Spacers have been crushed.
EHD44					sonication 5 min in acetone and IPA		13:00	No growth, No coalescence. Spacing too big.
EHD66	sonication 5 min in acetone and IPA. HMDS for 3h	PDMS			sonication 5 min in acetone and IPA. HMDS treated for 3h		20:00	Pillars have spanned the gap. Most seem to have broken when molten.
EHD68	sonication 5 min in acetone and IPA	ETFE	45,2	516	sonication 5 min in acetone and IPA. HMDS treated for 3h		17:50	Imprint destroyed. Substrates rotated during annealing.
EHD74		PDMS	32,2	369			16:20	No growth. Some coalescence.
EHD78*		ETFE					17:39	Fully developed pillars.
EHD81	sonication 5 min in acetone and IPA. HMDS for 3h	PDMS			sonication 5 min in acetone and IPA.			Short circuit, aborted
EHD82			21,5	246				Short circuit, aborted
EHD83*			32,2	369			02:30	Pillars have spanned the gap. Most seem to have broken when molten.
EHD84			21,5	246			16:30	Pillars have spanned the gap. Most seem to have broken when molten.
EHD84							16:15	Pillars have spanned the gap. Most seem to have broken when molten.
EHD87*		PDMS	21,5	246			02:00	Some fully developed pillars.

Table A.3: Experimental conditions and comments for annealed samples imprinted using molds with 4 µm diameter holes, continued from table A.2. Fully developed pillars have been measured for the plots on samples marked *

sample ID	substrate treatment before spin coating	mold	PS film thickness [nm]	imprinted pillar height [nm]	counter electrode treatment	voltage [V]	temperature [°C]	annealing time [hh:mm]	comments
EHD70	sonication 5 min in acetone and IPA.	PDMS	175	223	sonication 5 min in acetone and IPA.	50	190	00:48	Short circuit. Colloids crushed.
EHD71								63:30	Just a little bit of fully developed pillars along one edge.
EHD72*								16:13	Fully developed pillars.
EHD75*		ETFE	145,7	186	sonication 5 min in acetone and IPA. HMDS for 3h			04:00	Fully developed pillars.
EHD79*	sonication 5 min in acetone and IPA. HMDS for 3h	PDMS	160,9	205	sonication 5 min in acetone and IPA.			01:40	Fully developed pillars.
EHD88*	sonication 5 min in acetone and IPA.		73,4	93,5		55		04:00	Fully developed pillars.

Table A.4: Experimental conditions and comments for annealed samples imprinted using molds with 1.9 µm wide pyramidal holes

sample ID	substrate treatment before spin coating	mold	PS film thickness [nm]	counter electrode treatment	voltage [V]	temperature [°C]	annealing time [hh:mm]	comments
EHD48	sonication 5 min in acetone and IPA.	PDMS	21,5	sonication 5 min in acetone and IPA.	50	190	42:57	No coalescence, no growth
EHD49					100		02:05	No coalescence, no growth
EHD50			45,2				02:05	Short circuit
EHD51			73,4				01:20	No coalescence, no growth
EHD52					125		16:32	Short circuit
EHD53			98,7		50		15:31	Maybe some growth.
EHD54					75		16:09	Short circuit
EHD55			134,7		50		17:31	Maybe some growth.
EHD57	sonication 5 min in acetone and IPA. HMDS for 3h						15:21	Some growth evident from smaller base area.
EHD58	sonication 5 min in acetone and IPA.						19:49	Maybe some growth.
EHD67	sonication 5 min in acetone and IPA. HMDS for 3h						41:35	Some growth evident from smaller base area.
EHD85							68:06	Some growth evident from smaller base area.
EHD86					55		15:40	Some growth evident from smaller base area.